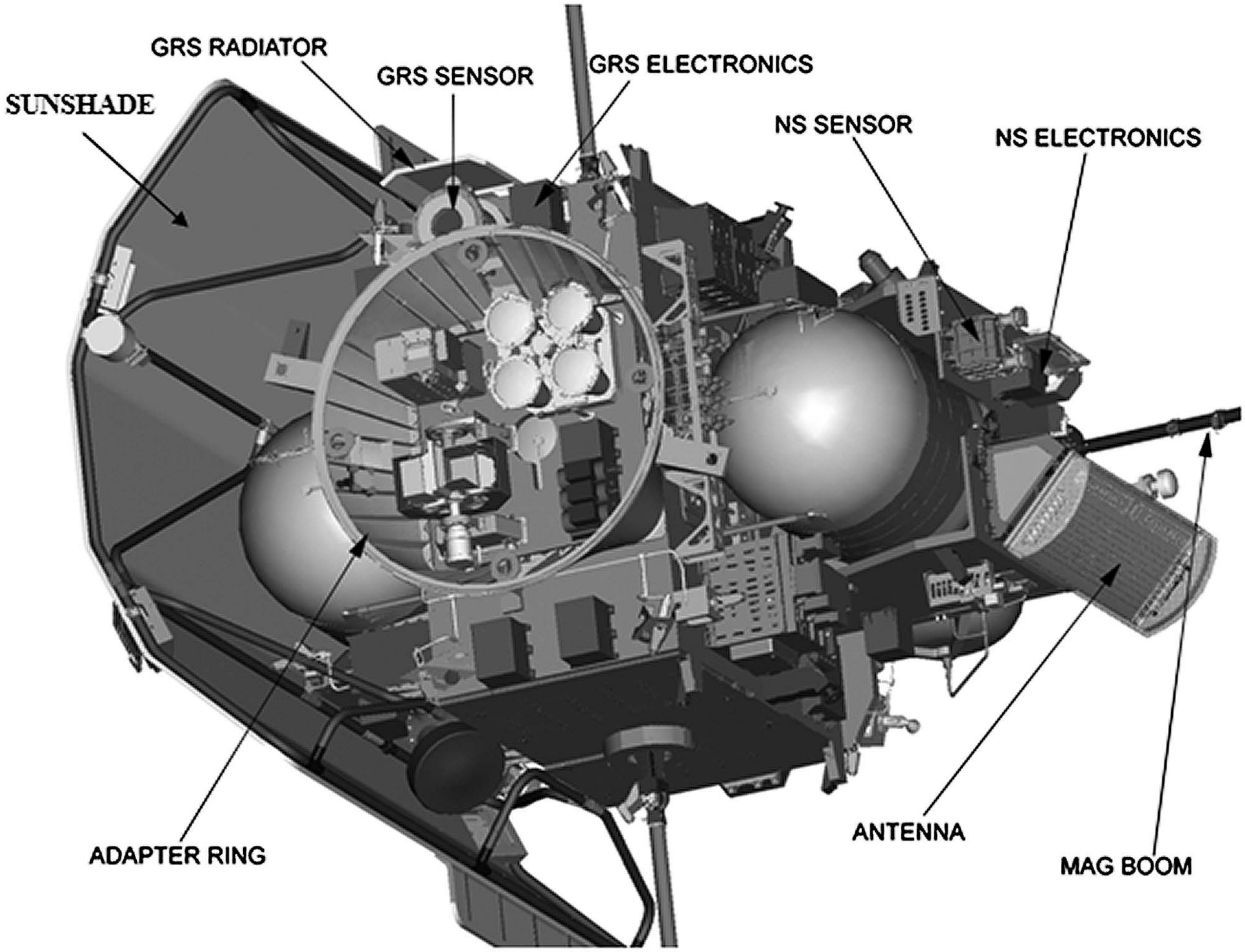

Figure A3. CAD drawing of GRS and NS as positioned on the MESSENGER spacecraft. Only a portion of the 3.6-m boom for MESSENGER's Magnetometer (MAG) is shown. Also indicated are one of MESSENGER's two high-gain phased-array antennas, the carbon fiber sunshade, and the adapter ring by which the spacecraft was mated to the upper stage of the launch vehicle. Figure reproduced from *Rhodes et al.* [2011].

these count rates originate from a large footprint on the surface, and therefore a wide range of θ_D angles. Despite this complication, the relationship between the count rates and θ_n (Figure A5) was found to closely match the relationship expected from the simulations, particularly that the count rate decreases for angles larger than ~45°, which is where the GRS-surrounding spacecraft components begin to attenuate the gamma-ray signal (Figure A4).

A5. GRS Point Response Function

[54] Use of the GRS efficiency maps in the forward code requires a means to properly weigh the relative contribution of any given point on the surface to the total measured gamma-ray count rate in the detector. This weighting was accomplished by utilizing a point response function (PRF) for the footprint of the GRS on the surface. The PRF was derived for an isotropic detector response, a uniform surface composition over the subtended limb solid angle, no atmosphere to attenuate gamma rays, and in the case of non-radioactive elements a constant neutron flux over depths penetrated by gamma rays. The assumption of an isotropic detector response was corrected through the use of the efficiency maps, which describe the non-uniform response of the detector. The PRF is energy-independent and uniform over all azimuth angles (ϕ_D). The PRF for a given point on the surface a distance d along the planet surface from the sub-nadir point is

$$\mathrm{PRF}(d) = \left[\frac{H^2(H - H'c)}{[H^2 + 2H'c]^{3/2}}\right] \qquad \text{(A1)}$$

where H is h/R_M, H' is $1 + H$, and c is $1 - \cos(d/R_M)$. The distance d is a function of the angle between the sub-nadir point and the surface component of interest, so the PRF for any angle can be calculated. The normalized PRF for each point d along the surface, corresponding to a specific detector-incident angle (θ_D, ϕ_D), was then calculated. The sum of the PRF-weighted detector efficiency at each incident angle multiplied by the altitude-corrected surface flux from